??????????????

(November 8, 2022)
GEO-Example
Running head: ***Geophysics* example**

ABSTRACT

Paleomagnetism is the main tool used in paleogeographic reconstructions, in which directional information of the past magnetic field is retrieved from ferromagnetic grains (l.s). Magnetic minerals have a wide range of size and composition that influence their magnetic properties and, consequently, their ability to record the directions of paleomagnetic fields. The signals obtained with classical paleomagnetic methodologies are vector averages that include all magnetic grains present in the samples, including the stable and unstable carriers. To improve the quality of the magnetic signal, it would be necessary to individually identify the magnetizations of the carriers of remanent magnetization, in order to isolate only the good registers of the geomagnetic field. This would allow obtaining more reliable paleomagnetic information, as well as possibly being effective for the paleomagnetic study of older rocks (e.g., Archean rocks), meteorites and even bodies with complex geological evolution. Therefore, this project aims to apply magnetic microscopy to identify the remanent magnetization directions of stable magnetic grains and, subsequently, invert these data in an attempt to recover the individual paleomagnetic directions of the magnetic carriers present in the thin-sections. If successful, a new precision methodology for paleomagnetic data acquisition will be implemented.

Keywords: Paleomagnetism, magnetic microscopy, Euler deconvolution, inversion of magnetic data.

INTRODUCTION

Paleomagnetism is the study of the record of the Earth's magnetic field preserved in rocks, being the main tool, and the only quantitative method, used during paleogeographic reconstruction (*Butler*, 1992). It is based on three basic assumptions: (i) the geomagnetic field can be approximated to the field created by a geocentric axial dipole (GAD) aligned with the Earth's axis of rotation over a period that eliminates paleosecular variation ($> 10^4$ years) (*McElhinny and McFadden*, 2000); (ii) ferromagnetic minerals (l.s.) acquire natural remanent magnetization (NRM) parallel to the Earth's geomagnetic field (*Dunlop and Özdemir*, 1997; *Tauxe et al.*, 2018); and (iii) this acquired magnetization is recorded for a long period of time, depending on the physicochemical characteristics of the magnetized mineral, following Neél's Theory (*Néel*, 1949, 1955) and being also influenced by the geological processes by which the rocks were submitted.

The thermoremanent magnetizations (TRMs) of magnetic particles in geological materials are the main records of the direction of the geomagnetic field of the past (*de Groot et al.*, 2014). Iron oxides, such as magnetite, which is the most common magnetic mineral present in rocks (*O'Reilly*, 1984) and acquire TRM as they cool below their Curie temperature and subsequently this direction of magnetization is "frozen" upon reaching blocking temperature (*Dunlop and Özdemir*, 1997). When the grains are small enough, and the magnetization is unidirectional homogeneous (single domain - SD), the acquisition and preservation of magnetic signals is physically supported by Néel's theory (*Néel*, 1949, 1955), conserving the remanent magnetization for long periods of time, on the order of billions of years, and for this reason, they are considered "good recorders" of the paleomagnetic field. In addition to SD, pseudo-single domain (PSD) particles, in the flower and stable

vortex states, can also preserve magnetization for periods on the order of the solar system age (*Nagy et al.*, 2017). On the other hand, Néel's theory does not cover larger particles (multi domain - MD), which have unstable remanent magnetization (e.g., caused by viscous reordering of magnetic domains, *de Groot et al.* (2014)), so they are particles with limited ability to record the geomagnetic field. In addition to the magnetic domain state, particles can still vary in composition, size and shape which causes changes in their magnetic properties. All these factors are crucial in determining stable remanence directions used in the calculation of paleomagnetic poles.

Classic techniques for obtaining paleomagnetic data, e.g., thermal demagnetization and alternating fields, are based on the progressive acquisition of the magnetization contained in cylindrical samples, usually of 10 cm^3. The magnetic signal of a single specimen is the result of the sum of moments contained in the assembly of ferromagnetic grains, including stable and unstable registers (*de Groot et al.*, 2021). although there are recent well-structured studies of imaging magnetic minerals in thin-sections (e.g., *Almeida et al.*, 2014; *Farchi et al.*, 2017; *Glenn et al.*, 2017; *Lima et al.*, 2014; *Lima and Weiss*, 2009; *Nichols et al.*, 2016; *Weiss et al.*, 2007; *de Groot et al.*, 2018, 2021), obtaining NRM directions of individual grains in the rock fabric remains, to the best of our knowledge, a challenge deeply explored only by *de Groot et al.* (2021). With the possibility of isolating the individual contributions of a fairly large number ($10^6 > N > 10^7$) of stable magnetic particles (SD/PSD) the magnetic directions recovered, using the average of their NRM vectors, would have an accurate paleomagnetic response (*Berndt et al.*, 2016), however such number of observations is unfeasible for the currently insufficient measurements scales of the equipaments (*de Groot et al.*, 2018).

Several branches of Earth Sciences have demonstrated the importance of the “spatiality" of data on a microscopic scale, mainly in Geochemistry and Geochronology, where it is possible to perform punctual analyzes and compositional maps, which allowed significant advances in the understanding of igneous, metamorphic and sedimentary processes (e.g., *Barnes et al.*, 2019; *Davidson et al.*, 2007; *Verberne et al.*, 2020). In Paleomagnetism there has been an interest in point magnetic analyses, or microscale magnetic maps, from magnetic microscopy techniques (*de Groot et al.*, 2014, 2018; *Lima et al.*, 2014; *Weiss et al.*, 2007). However, despite recent advances in this area, still there is no well-established inversion protocol to determine the magnetic vector direction of each individual ferromagnetic grains, nor the intensity of magnetization, without using additional information of the positioning and shape of these sources, such as micromagnetic tomography (e.g., *de Groot et al.*, 2018, 2021; *Fabian and De Groot*, 2019), which is a measurement spatially even more limited than the magnetic microscopy itself.

This paper aims to give a new perspective in the methodological routine that carry out paleomagnetic studies in microscale allowing to retrieve the individual remanent magnetization direction of these stable magnetic carriers (SD and PSD), semi automatically and without any additional information. In this way, a larger area of the thin section can be scanned with the objective of increasing the number of observations and, therefore, increasing the reliability of the directional data obtained. We also intend to generate a micromagnetic analysis protocol in an open source software, based on the techniques that will be described below.

METHODOLOGY

Scanning Magnetic Microscopy

Scanning magnetic microscopy (SMM) is the imaging technique in which a thin-section sample of geological material is horizontally displaced under a high-precision (fixed) micromagnetometer to obtain magnetization (*Weiss et al.*, 2007). The SMM performed at a fixed height above the sample also has the advantage of facilitating the subtraction of the ambient field (constant), to which it might be subject during the scan (*Lima et al.*, 2013). The availability of high-performance and low-cost magnetic sensors has promoted a great advance in the application of SMM in recent years. However, its sensitivity is still a few orders of magnitude lower than that of superconducting quantum interference devices (SQUIDs), the latter being between 10^{-12} and 10^{-15} Am^2 (*Lima et al.*, 2013). This disadvantage is offset by (i) the high spatial resolution of the SMM, as it is performed at a few tens of micrometers from the sampled surface; and (ii) SQUID magnetic microscopy is performed at low temperatures ($<$ 100K), which can cause changes in the original NRM of the sample, while SMM is performed at room temperature (*Lima et al.*, 2013; *Weiss et al.*, 2007).

The SMM can also be considered as a form of aeromagnetic survey, carried out at microscales on sources of flat topography, with high spatial resolution and greater sensitivity to magnetic moment (*Lima et al.*, 2013). An emerging magnetic imaging technology is the quantum diamond microscope (QDM) with very high spatial resolution ($\cong$ 1 µm), and can recover magnetic moments as weak as 10^{-17} Am^2, through magnetic sensors located at altitudes between 1 and 5 μm relative to the sample surface (*Fu et al.*, 2020) capable of detecting the magnetic signals of SD

magnetite particles (Figure 1). Another promising type of magnetic microscope is the magnetic tunnel junction (MTJ) with a spatial resolution greater than 7 μm, a magnetic moment sensitivity of up to 10^{-14} Am^2 and sample-sensor distance of 7 μm. Its advantages reside in the fact that these MTJ devices do not require high bias current to operate (few tens of μA), which avoids induced magnetization signals created by artificial magnetic field during the measurements (*Lima et al.*, 2014).

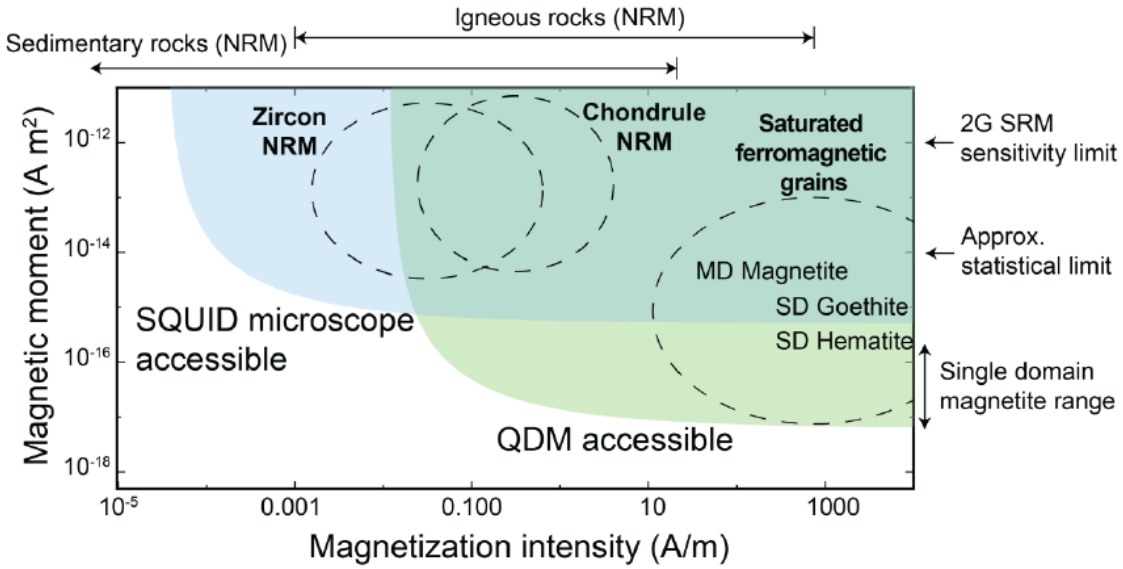

Figure 1: Sample classes accessible to QDM, SQUID microscope and 2G Enterprises SRM. The accessible region for the QDM was calculated assuming a magnetic field noise threshold of 5 nT and a minimum sensor-sample distance of 5 µm. The calculation for the SQUID microscope assumed field noise values of 15 pT and sensor-sample distance of 150 µm. Source: *Fu et al.* (2020).

Due to the similarities between magnetic microscopy techniques and aeromagnetic surveys, the methodologies of data inversion of the latter, densely studied in the last decades, can be adapted for magnetic microscopy. However, *Lima et al.* (2013) report important distinctions between SMM and aeromagnetic surveys, namely: (i) the source distribution in the SMM can often be accurately modeled in a

two-dimensional model; (ii) the SMM measures the field produced directly by the sample's NRM; (iii) the sensor positioning is very accurate in the SMM, and the vertical component of the magnetic field is usually measured, rather than the total field; (iv) there is no need for correction to bring all measurements to the same surface or to grid the data; and (v) the distributions of the magnetization sources are finite and known.

Euler Deconvolution

Euler Deconvolution is a consolidated method classically applied to data from aeromagnetic surveys. Given the similarities between SMM and aeromagnetic data, its application becomes plausible for determining the positions of magnetic sources caused by ferromagnetic minerals (l.s). Euler deconvolution is one of the most useful methods for estimating the three-dimensional positioning of magnetic sources/geological bodies (*Reid et al.*, 1990; *Thompson*, 1982). It is the application of a mobile operator in a small data window over the sampled data set. The observations made within this window are used to estimate the horizontal and vertical positions of the source by solving a small linear system of equations using the gradients of the potential field, provided that the shapes of the sources are assumed.

Despite this, this system usually has a large number of solutions (*Barbosa and Silva*, 2011), which becomes a limitation for the method. In an attempt to circumvent the problem of this expressive cloud of solutions, we suggest the previous application of a method of delimitation of the contours of the sources generating the potential field and later the application of Euler's Deconvolution, which becomes unique for

each source (one data window per source). As the method itself already requires the gradients of the potential field, therefore, the method of delimitation chosen was the horizontal gradient (*Cordell and Grauch*, 1982). *Blakely* (1996) states that the response of a source's horizontal gradient tends to overlap its limits, thus obtaining a two-dimensional robust map of the sources location. The amplitude of the horizontal gradient (∇H) is expressed by Equation (1). Once the source positions are determined by this preliminary method then, subsequently, Euler Deconvolution is applied and a static window for each source generating the potential field.

$$\nabla H = \sqrt{\left(\frac{\partial F}{\partial x}\right)^2 + \left(\frac{\partial F}{\partial y}\right)^2} \tag{1}$$

Euler Deconvolution Formulation

The anomaly of a potential field F produced by a three-dimensional source, whose cartesian coordinates of its central position are x_0, y_0 and z_0, satisfies the homogeneous Euler equation (*Reid et al.*, 1990) expressed by:

$$(x - x_0) \cdot \frac{\partial F}{\partial x} + (y - y_0) \cdot \frac{\partial F}{\partial y} + (z - z_0) \cdot \frac{\partial F}{\partial z} = n \cdot (b - F) \tag{2}$$

where: n is the structural index, that is, a gauge of the geometric shape of the sources causing the anomaly; and b is the constant, and unknown, base level.

The Euler's Deconvolution uses the gradient of a potential field and the structural index, which can be defined by the geometric nature of the sources. The structural index is the only necessary a priori knowledge. Once a value for n is assumed (n

= 3 for spherical/punctual magnetic sources), the homogeneous Euler equation can be rearranged as follows:

$$x_0 \cdot \frac{\partial F}{\partial x} + y_0 \cdot \frac{\partial F}{\partial y} + z_0 \cdot \frac{\partial F}{\partial z} + n \cdot b = x \cdot \frac{\partial F}{\partial x} + y \cdot \frac{\partial F}{\partial y} + z \cdot \frac{\partial F}{\partial z} + n \cdot F \tag{3}$$

The Equation (3) can be written in matrix form as:

$$\begin{bmatrix} Fx_1 & Fy_1 & Fz_1 & n \\ Fx_2 & Fy_2 & Fz_2 & n \\ \vdots & \vdots & \vdots & \vdots \\ Fx_N & Fy_N & Fz_N & n \end{bmatrix} \begin{bmatrix} x_0 \\ y_0 \\ z_0 \\ b \end{bmatrix} = \begin{bmatrix} x_1 \cdot Fx_1 + y_1 \cdot Fy_1 + z_1 \cdot Fz_1 + n \cdot F_1 \\ x_2 \cdot Fx_2 + y_2 \cdot Fy_2 + z_2 \cdot Fz_2 + n \cdot F_2 \\ \vdots \\ x_N \cdot Fx_N + y_N \cdot Fy_N + z_N \cdot Fz_N + n \cdot F_N \end{bmatrix} \tag{4}$$

Where: Fx_i, Fy_i and Fz_i represent, respectively, the gradients $\frac{\partial F}{\partial x}$, $\frac{\partial F}{\partial y}$ and $\frac{\partial F}{\partial z}$ evaluated on the i-th observation point ($i = 1, 2, ..., N$). While x_i, y_i and z_i represent the cartesian coordinates at the i-th observation point.

Note that Equation (4) is a linear system $\bar{\bar{G}} \cdot \bar{m} = \bar{d}$ and its objective function $f(\bar{m})$ expressed by:

$$f(\bar{m}) = \|e\|^2 = (\bar{\bar{G}} \cdot \bar{m} - \bar{d})^T \cdot (\bar{\bar{G}} \cdot \bar{m} - \bar{d}) \tag{5}$$

The solution $\bar{m}$ of the system can be obtained by minimizing the objective function ($\frac{\partial f}{\partial m_k} = \bar{0}$) through the least squares estimator given by:

$$\bar{m} = \left(\bar{\bar{G}}^T \cdot \bar{\bar{G}}\right)^{-1} \cdot \left(\bar{\bar{G}}^T \cdot \bar{d}\right) \tag{6}$$

Thus, $\bar{m} = [x_0 \;\; y_0 \;\; z_0 \;\; b]^T$ will be the solution vector that satisfies Euler's Equation with the least possible error containing the position coordinates font center (x_0, y_0, z_0) and the base level (b).

Magnetic Inversion

The rapid inversion of the total field is a method developed by *Oliveira Jr. et al.* (2015) being computationally efficient to invert the magnetic anomalies produced by multiple sources with approximately spherical shapes to estimate their magnetization directions (inclination and declination). This methodology requires the central position of the magnetic sources, which can be obtained with Euler Deconvolution, and the information on their geometry helps to reduce the non-exclusivity of the problem. In this way, it is possible to estimate the direction of magnetization from multiple sources. The method does not require that all sources have the same magnetization direction nor the use of regularly spaced data on a horizontal grid, and can still be implemented in linear and non-linear inversion problems.

Currently, the main inversion limitations for these type of data are: (i) in part because the sampling scale during measurement is insufficiently accurate and (ii) because of the non-singularity of the magnetic inversion (*Lima et al.*, 2013). The basic mathematical structure associated with the inverse problem of aeromagnetic data can be adapted and used in SMM data due to its similarity, despite the

non-singularity caused by the infinite number of solutions for the same observed magnetic field (*Weiss et al.*, 2007). Assigning as much information as possible about the analyzed sample and the experimental environment can reduce this ambiguity by recovering the magnetization direction. In particles with unidirectional magnetization, and without magnetization sources outside the sample area, it is possible to guarantee singularity for the inverse problem in SMM (*Baratchart et al.*, 2013). Associating the fact that there is a singularity in the response of uniformly magnetized particles and that ferromagnetic particles (*l.s.*) with stable magnetization have such a characteristic, therefore, the inversion method becomes ideal for the purpose of this project.

Parametrization and Forward Model

Let $\bar{B}$ be the observed data vector, whose i-th element $\bar{B}_i$, $i = 1, 2, ..., N$, is a total field anomaly, resulting from the NRM contribution of each ferromagnetic particle (*l.s.*), measured at position (x_i, y_i, z_i) (black dots, Figure 2). In this cartesian coordinate system, x points to geographic north, y points east, and z points down. In general, the magnetic field that is produced in the thin section is the result solely and exclusively of the NRM contribution of the particles without considering the induced component, since the measurements carried out in the magnetic microscope are usually made under magnetic shielding conditions. Thereby, approximating the shape of ferromagnetic minerals (*l.s.*) to NRM magnetizing spheric/punctual sources. According to *Blakely* (1996) the equation of a uniformly magnetized sphere is given by:

$$b = C_m \cdot \frac{4}{3} \cdot \pi \cdot R^3 \cdot m \cdot \hat{m} \cdot \frac{1}{r^2} \cdot \hat{r} \tag{7}$$

Whereas the magnetic sources can be represented by a set of L uniformly magnetized spheres. In this case, each sphere will have a contribution in the field measured at the position (x_i, y_i, z_i):

$$b_i{}^j = C_m \cdot \frac{4}{3}\pi \cdot R_j{}^3 \cdot \bar{m}^j \cdot \frac{1}{r_{i,j}^2} \cdot \hat{r}_{i,j} \ , \quad j = 1,\ 2 \ldots,\ L \tag{8}$$

Where: $C_m = \frac{\mu_0}{4\pi} = 10^{-7}\frac{H}{m}$; R_j is the radius of the j-th sphere; $r_{i,j}$ is the distance (unit vector $\hat{r}_{i,j}$) between the center of the j-th sphere and the observation point i, i = 1, 2, . .. N; and $\bar{m}^j = \left[mx_j\ my_j\ mz_j\right]^T$ is the vector formed by the cartesian components of the magnetization of the j-th sphere (unit vector $\hat{m}^j$).

Thus, the total magnetization measured at the position (x_i, y_i, z_i) will be the sum of contributions from the L spheres, given by:

$$B_i = \sum_{j=1}^{L} b_i^j \tag{9}$$

According to *Oliveira Jr. et al.* (2015) the Equation (8) can be segmented into two members: (i) the first being a matrix M_i^j encompassing the vector relationship with the positioning for each source and (ii) the second being h_j, which is the vector that encompasses the cartesian components of the magnetization of each sphere:

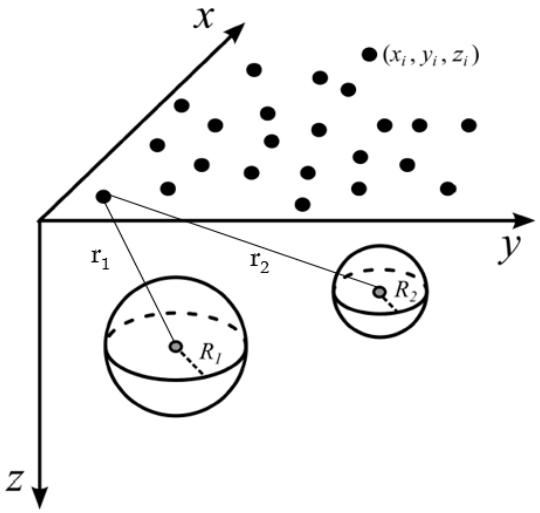

Figure 2: Schematic representation of spheres (L = 2) uniformly magnetized in the subsurface, whose magnetic effect, produced by these spheres, can be observed at points (x_i, y_i, z_i), i = 1, 2, ..., N (points black). In this cartesian coordinate system, x points to geographic north, y points east, and z points down. Modified from: *Oliveira Jr. et al.* (2015).

$$M_i^j = \begin{bmatrix} \left(\frac{\partial^2}{\partial x \partial x} \cdot \frac{1}{r_{i,j}}\right) & \left(\frac{\partial^2}{\partial x \partial y} \cdot \frac{1}{r_{i,j}}\right) & \left(\frac{\partial^2}{\partial x \partial z} \cdot \frac{1}{r_{i,j}}\right) \\ \left(\frac{\partial^2}{\partial x \partial y} \cdot \frac{1}{r_{i,j}}\right) & \left(\frac{\partial^2}{\partial y \partial y} \cdot \frac{1}{r_{i,j}}\right) & \left(\frac{\partial^2}{\partial x \partial z} \cdot \frac{1}{r_{i,j}}\right) \\ \left(\frac{\partial^2}{\partial x \partial z} \cdot \frac{1}{r_{i,j}}\right) & \left(\frac{\partial^2}{\partial y \partial z} \cdot \frac{1}{r_{i,j}}\right) & \left(\frac{\partial^2}{\partial z \partial z} \cdot \frac{1}{r_{i,j}}\right) \end{bmatrix}_{3N \times 3L}, h_j = \begin{bmatrix} mx_j \,.C_m \cdot \frac{4}{3}\pi \cdot R_j^3 \\ my_j \,.C_m \cdot \frac{4}{3}\pi \cdot R_j^3 \\ mz_j \,.C_m \cdot \frac{4}{3}\pi \cdot R_j^3 \end{bmatrix}_{3L \times 1} \tag{10}$$

$$\text{Where: } \frac{1}{r_j} \equiv \frac{1}{\sqrt{\left(x_i - xc_j\right)^2 + \left(y_i - yc_j\right)^2 + \left(z_i - zc_j\right)^2}}$$

Subsequently, the components of the total magnetizing field can be obtained (from Equation (9)), as shown below:

$$\begin{bmatrix} \left(\frac{\partial^2}{\partial x \partial x} \cdot \frac{1}{r_{i,j}}\right) & \left(\frac{\partial^2}{\partial x \partial y} \cdot \frac{1}{r_{i,j}}\right) & \left(\frac{\partial^2}{\partial x \partial z} \cdot \frac{1}{r_{i,j}}\right) \\ \left(\frac{\partial^2}{\partial x \partial y} \cdot \frac{1}{r_{i,j}}\right) & \left(\frac{\partial^2}{\partial y \partial y} \cdot \frac{1}{r_{i,j}}\right) & \left(\frac{\partial^2}{\partial x \partial z} \cdot \frac{1}{r_{i,j}}\right) \\ \left(\frac{\partial^2}{\partial x \partial z} \cdot \frac{1}{r_{i,j}}\right) & \left(\frac{\partial^2}{\partial y \partial z} \cdot \frac{1}{r_{i,j}}\right) & \left(\frac{\partial^2}{\partial z \partial z} \cdot \frac{1}{r_{i,j}}\right) \end{bmatrix}_{3N \times 3L} \cdot \begin{bmatrix} mx_j \,.C_m \cdot \frac{4}{3}\pi \cdot R_j^3 \\ my_j \,.C_m \cdot \frac{4}{3}\pi \cdot R_j^3 \\ mz_j \,.C_m \cdot \frac{4}{3}\pi \cdot R_j^3 \end{bmatrix}_{3L \times 1} = \begin{bmatrix} Bx_i \\ By_i \\ Bz_i \end{bmatrix}_{3N \times 1} \tag{11}$$

As in the specific case in the study of magnetic microscopy, in the routine practice, the vertical component of magnetization is usually measured. In this case, there is a need to adapt the Equation (11) to isolate the response from the vertical component (B_z). Therefore, the equation of the direct model will be given by:

$$\left[\left(\frac{\partial^2}{\partial x \partial z}\cdot\frac{1}{r_{i,j}}\right)\quad\left(\frac{\partial^2}{\partial y \partial z}\cdot\frac{1}{r_{i,j}}\right)\quad\left(\frac{\partial^2}{\partial z \partial z}\cdot\frac{1}{r_{i,j}}\right)\right]_{\mathrm{N}\times 3\mathrm{L}}\cdot\begin{bmatrix} mx_j \,.C_m\cdot\frac{4}{3}\pi\cdot R_j^3 \\ my_j \,.C_m\cdot\frac{4}{3}\pi\cdot R_j^3 \\ mz_j \,.C_m\cdot\frac{4}{3}\pi\cdot R_j^3 \end{bmatrix}_{3\mathrm{L}\times 1} = [\,Bz_i\,]_{\mathrm{N}\times 1} \tag{12}$$

The magnetization is usually represented in spherical coordinates of intensity (Q (A/m)), declination (D (°)) and inclination (I (°)). Thus, the vector $\bar{m}_j$, containing the cartesian coordinates of magnetization, of the direct model can also be calculated as follows:

$$\begin{bmatrix} mx_j \\ my_j \\ mz_j \end{bmatrix}_{3\mathrm{L}\times 1} = Q_j\cdot\begin{bmatrix} cos\left(I_j\right)\cdot cos\left(D_j\right) \\ cos\left(I_j\right)\cdot sin\left(D_j\right) \\ sin\left(I_j\right) \end{bmatrix}_{3\mathrm{L}\times 1} \tag{13}$$

We can simplify the Equation (12) to:

$$\left[\left(\frac{\partial^2}{\partial x \partial z}\cdot\frac{1}{r_{i,j}}\right)\quad\left(\frac{\partial^2}{\partial y \partial z}\cdot\frac{1}{r_{i,j}}\right)\quad\left(\frac{\partial^2}{\partial z \partial z}\cdot\frac{1}{r_{i,j}}\right)\right]_{\mathrm{N}\times 3\mathrm{L}}\cdot\begin{bmatrix} hx_j \\ hy_j \\ hz_j \end{bmatrix}_{3\mathrm{L}\times 1} = [\,Bz_i\,]_{\mathrm{N}\times 1} \tag{14}$$

With this, the Equation (14) can be rewritten in linear form, given by:

$$\bar{\bar{M}}\cdot\bar{h}_j = \bar{B}_z \tag{15}$$

Inverse Model

Assuming that the ferromagnetic minerals (*l.s.*) that give rise to the observed magnetization component data vector $\bar{B}_z$ can be approximated by a set of L uniformly magnetized spheres with known coordinates (xc_j, yc_j, zc_j), j = 1, 2, ..., L, of their centers. Also assuming that there is no induced magnetization component, only that of the NRM. Under these assumptions, a superdetermined inverse linear problem is formulated to estimate the vector of parameters $\bar{h}$ (Equation (15)) from the observed data $\bar{B}_z$ and $\bar{\bar{M}}$, the latter being obtained previously with the Euler Deconvolution.

The problem of estimating a parameter vector $\bar{h}$ containing the spheres' magnetization vectors can be solved by minimizing the objective function $f\left(\bar{h}\right)$:

$$f\left(\bar{h}\right) = \|e\|^2 = e^T \cdot e = \left(\bar{\bar{M}} \cdot \bar{h} - \bar{d}\right)^T \cdot \left(\bar{\bar{M}} \cdot \bar{h} - \bar{B}_z\right) \tag{16}$$

When differentiating the (Equation (16)) by $\bar{h}$ and equating the result to the zero vector ($\frac{\partial f}{\partial h_k} = \bar{0}$). Then we obtain the normal equation for estimating least squares solution given by:

$$\bar{h} = \left(\bar{\bar{M}}^T \cdot \bar{\bar{M}}\right)^{-1} \cdot \left(\bar{\bar{M}}^T \cdot \bar{B}_z\right) \tag{17}$$

As the least squares estimate (Equation (17)) is very sensitive to the presence of outliers in the observed data, the estimated parameters could be seriously misleading. To counteract this problem *Oliveira Jr. et al.* (2015) suggest a robust scheme based on the minimization of the objective function obtained with the absolute error:

$$f\left(\widetilde{h}\right) = \left(\sum_{i=1}^{N} \left| \left(\bar{\bar{M}} \cdot \bar{h}\right)_i - (\bar{B}_z)_i \right| \right) \tag{18}$$

Unlike the solution presented for the objective function in Equation (17), the parameter vector minimizing Equation (18) cannot be obtained as a simple linear system. A practical way is the iteratively reweighted least squares algorithm (*Aster et al.*, 2019; *Oliveira Jr. et al.*, 2015). In this algorithm, at each iteration k, the following linear system is solved:

$$\widetilde{h}^{k+1} = \left(\bar{\bar{M}}^T \cdot \bar{\bar{R}}^k \cdot \bar{\bar{M}}\right)^{-1} \cdot \left(\bar{\bar{M}}^T \cdot \bar{\bar{R}}^k \cdot \bar{B}_z\right) \tag{19}$$

The term $\bar{\bar{R}}^k$ is an N $\times$ N diagonal matrix whose i-th element r_i^k (i = 1, 2, ..., N) is given by:

$$r_i{}^k = \frac{1}{\left| \left(\bar{\bar{M}} \cdot \bar{h}\right)_i - \bar{B}_{zi} + e \right|} \tag{20}$$

Where: e is a small positive number used to prevent singularities

This iterative process starts (k = 0) with the solution vector obtained by the least squares estimator (Equation (17)). From this initial approximation $\widetilde{h}^0$, we calculate the matrix $\bar{\bar{R}}^0$ (Equation (20)). Which is used in the solution of the linear system given by Equation (19) to obtain the estimate $\widetilde{h}^1$. Later using this updated estimate to calculate the new matrix $\bar{\bar{R}}^1$ (Equation (20)), we solve the linear system (Equation (19)) to obtain a new estimate $\widetilde{h}^2$, and so on. As the iterations progress, this iterative procedure tends to converge and estimate $\widetilde{h}$, which is called robust estimate (*Oliveira Jr. et al.*, 2015). According to *Aster et al.* (2019) this convergence can be limited by a tolerance τ, given by:

$$\frac{\|\widetilde{h}^{k+1} - \widetilde{h}^{k}\|}{1 + \|\widetilde{h}^{k+1}\|} \leq \tau \tag{21}$$

Where: τ is a positive number (*e.g.*, 10^{-2}) chosen by the algorithm user.

Directions of Magnetization and Uncertainty Propagation

In paleomagnetic studies the magnetization vectors are represented in terms of their declination (D) and inclination (I). These are given as a function of the magnetization vector $\bar{h}_j$ (Equation (14)) and represented in spherical coordinates (as shown in Figure 3).

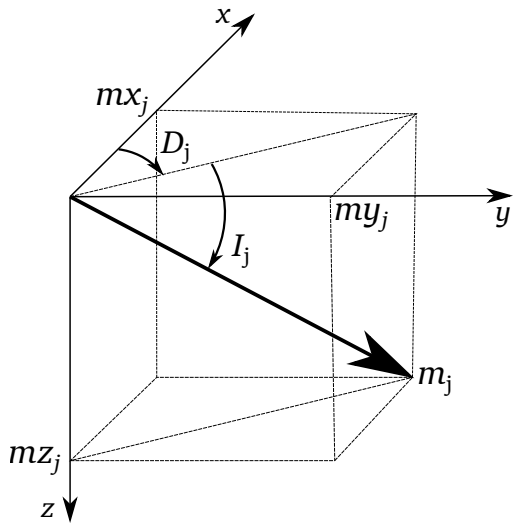

Figure 3: Schematic representation of vector h_j (Equation (14)) with elements hx_j, hy_j and hz_j in cartesian coordinates. This vector has declination D_j (positive clockwise) and slope I_j (positive downwards), j = 1, 2, ... L. Source: *Oliveira Jr. et al.* (2015).

In this way, it is possible to determine the magnetization directions D_j and I_j for the j-th sphere of the set of L spheres by using:

$$D_j = \tan^{-1}\left(\frac{hy_j}{hx_j}\right) \tag{22}$$

$$I_j = \tan^{-1}\left(\frac{hz_j}{\sqrt{\left(hx_j\right)^2 + \left(hy_j\right)^2}}\right) \tag{23}$$

In a micromagnetic survey, or any geophysical survey, measurements are affected by noise caused by experimental errors and equipment inaccuracies. Noise in the observed data vector $\bar{B}_z$ affects the solution of the estimated parameter vector $\bar{h}_j$, regardless of the method used. Assuming that the noise during the measurement of the observed data is independent and with variance ${\sigma_0}^2$, one can quantify this effect on the estimated parameters through propagation of the covariance (*Aster et al.*, 2019). The covariance matrix of these parameters will be given by:

$$\bar{\bar{Cov}}\left(\bar{h}_j\right) = {\sigma_0}^2 \cdot \left(\bar{\bar{M}}^T \cdot \bar{\bar{M}}\right)^{-1} \quad (\textit{least square}) \tag{24}$$

$$\bar{\bar{Cov}}\left(\widetilde{h}_j\right) = {\sigma_0}^2 \cdot \left(\bar{\bar{M}}^T \cdot \bar{\bar{R}}^k \cdot \bar{\bar{M}}\right)^{-1} \quad (\textit{robust}) \tag{25}$$

The main diagonal of the covariance matrix (Equation (24) and Equation (25)) contains the variance of each member of the parameter vector, as expressed below:

$$\bar{\bar{Cov}} = \begin{bmatrix} Var(hx_1) & \cdots & \cdots & \cdots & \cdots & \cdots & \cdots \\ \cdots & Var(hy_1) & \cdots & \cdots & \cdots & \cdots & \cdots \\ \cdots & \cdots & Var(hz_1) & \cdots & \cdots & \cdots & \cdots \\ \cdots & \cdots & \cdots & \ddots & \cdots & \cdots & \cdots \\ \cdots & \cdots & \cdots & \cdots & Var(hx_L) & \cdots & \cdots \\ \cdots & \cdots & \cdots & \cdots & \cdots & Var(hy_L) & \cdots \\ \cdots & \cdots & \cdots & \cdots & \cdots & \cdots & Var(hz_L) \end{bmatrix}_{3L \times 3L} \tag{26}$$

Thus, for the j-th sphere:

$$\sigma_{hx_j} = \sqrt{Var(hx_j)}, \quad \sigma_{hy_j} = \sqrt{Var(hy_j)} \quad \text{and} \quad \sigma_{hz_j} = \sqrt{Var(hz_j)} \tag{27}$$

Thus, the propagation of uncertainties of the declination (D_j) and slope (I_j) results are given as a function of the parameters obtained in Equation (27):

$$\sigma_{D_j} = \sqrt{\left(\frac{\partial D_j}{\partial hx_j}\right)^2 \cdot \left(\sigma_{hx_j}\right)^2 + \left(\frac{\partial D_j}{\partial hy_j}\right)^2 \cdot \left(\sigma_{hy_j}\right)^2} \tag{28}$$

$$\sigma_{I_j} = \sqrt{\left(\frac{\partial I_j}{\partial hx_j}\right)^2 \cdot \left(\sigma_{hx_j}\right)^2 + \left(\frac{\partial I_j}{\partial hy_j}\right)^2 \cdot \left(\sigma_{hy_j}\right)^2 + \left(\frac{\partial I_j}{\partial hz_j}\right)^2 \cdot \left(\sigma_{hz_j}\right)^2} \tag{29}$$

Where:

$$\frac{\partial D_j}{\partial hx_j} = \frac{-hy_j}{{hx_j}^2 + {hy_j}^2} \tag{30}$$

$$\frac{\partial D_j}{\partial hy_j} = \frac{hx_j}{hx_j{}^2 + hy_j{}^2} \tag{31}$$

$$\frac{\partial I_j}{\partial hx_j} = \frac{-hx_j \cdot \ hz_j}{\sqrt{hx_j{}^2 + hy_j{}^2} \cdot \left(hx_j{}^2 + hy_j{}^2 + hz_j{}^2\right)} \tag{32}$$

$$\frac{\partial I_j}{\partial hy_j} = \frac{-hy_j \cdot \ hz_j}{\sqrt{hx_j{}^2 + hy_j{}^2} \cdot \left(hx_j{}^2 + hy_j{}^2 + hz_j{}^2\right)} \tag{33}$$

$$\frac{\partial I_j}{\partial hz_j} = \frac{\sqrt{hx_j{}^2 + hy_j{}^2}}{\left(hx_j{}^2 + hy_j{}^2 + hz_j{}^2\right)} \tag{34}$$

RESULTS

Synthetic Data

We applied the proposed method in a numerical simulation of a geological thin-section of dimensions 1000 µm x 1000 µm in a regular grid (1000 x 1000) for estimating the magnetization directions of four spherical sources uniformly magnetized (but different directions), according to Table 1. Totaling an observation number N = 10^6 obtained at a sensor-sample distance of 5 µm and a spacing of 1 µm. Subsequently, a pseudorandom noise of normal Gaussian distribution, with a zero mean and standard variation $\cong$ 5% of the anomaly amplitude, was added to the data as shown in Figure XX.

Table 1: Initial position and magnetization parameters for each spherical source.

Sphere	Center coordinates			Magnetization		
	X (μm)	Y (μm)	Z (μm)	Q (A/m)	D (°)	I (°)
1	250	250	8.50	6.0	-140	-30
2	500	500	10.0	6.0	0	62
3	750	750	5.30	6.0	-70	-50
4	200	800	7.75	6.0	125	22

Euler Solution

The first step is to calculate the magnetic horizontal gradient in order to isolate the window data of each source. In the horizontal gradient, the magnetic anomaly caused by a body tends to overlap its limits, thus obtaining a robust positioning (*Blakely*, 1996). *van der Walt et al.* (2014).

Table 2: Central positions of sources input vs Euler deconvolution solutions.

Esfera	Posição do Centro de Entrada			Solução de Euler		
	X (μm)	Y (μm)	Z (μm)	X (μm)	Y (μm)	Z (μm)
1	250	250	8.50	249.144984	250.084691	8.17863468
2	500	500	10.0	500.213134	500.443637	9.85904976
3	750	750	5.30	749.873747	750.127834	5.26685529
4	200	800	7.75	200.177971	800.331017	7.82974687

Table 3: Input magnetization directions vs inversion solutions and their error propagation.

Esfera	Direção de Entrada		Direções Recuperadas e Incertezas			
	D (°)	I (°)	D (°)	σ D (°)	I (°)	σ I (°)
1	-140	-30	-137.0294	$\pm$ 0.7641	-32.6550	$\pm$ 0.5169
2	0	62	2.5167	$\pm$ 1.5004	60.5473	$\pm$ 0.6917
3	-70	-50	-68.3316	$\pm$ 0.6752	-49.0172	$\pm$ 0.3923
4	125	22	124.8320	$\pm$ 0.6449	21.9940	$\pm$ 0.4515

DISCUSSION

CONCLUSION

We developed an efficient semi-automated method to determine the direction of magnetization of dipolar sources on a microscale, as well as the recovery of their magnetic moment. Being ideal for a reinterpretation for the application of methods of paleomagnetic studies using thin sections of rock samples. This would be an attempt to improve the quality of results obtained by isolating the responses of more reliable recorders of the Earth's geomagnetic field.

We also present a new, faster and cleaner way to solve the Euler equation in determining the positioning of magnetic anomaly sources using a pre-selection of magnetic anomaly source windows based on the Laplacian of the Gaussian applied to total gradient anomaly maps. In this way, reducing the numerous solutions to just one data window per source. After estimating the structural index (N=3) by approximating the sources generating the magnetic anomaly to spheres/points, the Euler deconvolution is performed and the central position of each source is determined.

Since for the recovery of direction and magnetization we only need to assume that the sources have their central positions known (so we apply Euler deconvolution) and that their magnetizations are uniform. This last premise aligns with the theory of magnetically stable particles, which are the basis of classical paleomagnetism. Also, there is no need for any kind of prior knowledge other than the observed magnetic anomaly, and the structural index of the sources. Therefore, this method can be quickly replicated in a dataset of thin sections of rocks to obtain the

distributions of magnetic directions of each source identified in the sample.

The test using a simply synthetic sample shows the great capability of the method by retrieving not only the precisely center positions

REFERENCES

Almeida, T. P., T. Kasama, A. R. Muxworthy, W. Williams, L. Nagy, and R. E. Dunin-Borkowski, Observing thermomagnetic stability of nonideal magnetite particles: Good paleomagnetic recorders?, *Geophysical Research Letters*, *41*(20), 7041–7047, doi:10.1002/2014GL061432, 2014.

Aster, R. C., B. Borchers, and C. H. Thurber, *Parameter Estimation and Inverse Problems*, Elsevier, San Diego, USA, doi:10.1016/C2015-0-02458-3, 2019.

Baratchart, L., D. P. Hardin, E. A. Lima, E. B. Saff, and B. P. Weiss, Characterizing kernels of operators related to thin-plate magnetizations via generalizations of Hodge decompositions, *Inverse Problems*, *29*(1), 015,004, doi:10.1088/0266-5611/29/1/015004, 2013.

Barbosa, V. C., and J. B. Silva, Reconstruction of geologic bodies in depth associated with a sedimentary basin using gravity and magnetic data, *Geophysical Prospecting*, *59*(6), 1021–1034, doi:10.1111/j.1365-2478.2011.00997.x, 2011.

Barnes, C., J. Majka, D. Schneider, K. Walczak, ·. Michał Bukała, K. Kośmińska, T. Tokarski, and A. Karlsson, High-spatial resolution dating of monazite and zircon reveals the timing of subduction-exhumation of the Vaimok Lens in the Seve Nappe Complex (Scandinavian Caledonides), *Contributions to Mineralogy and Petrology*, *174*, 5, doi:10.1007/s00410-018-1539-1, 2019.

Berndt, T., A. R. Muxworthy, and K. Fabian, Does size matter? Statistical limits of paleomagnetic field reconstruction from small rock specimens, *Journal of Geophysical Research: Solid Earth*, *121*(1), 15–26, doi:10.1002/2015JB012441, 2016.

Blakely, R. J., *Potential Theory in Gravity and Magnetic Applications*, 461 pp., Cambridge University Press, Cambridge, 1996.

Butler, R. F., *Paleomagnetism: magnetic domains to geologic terranes*, 238 pp., Blackwell Scientific Publications, Boston, doi:10.5860/choice.29-5708, 1992.

Cordell, L., and V. I. Grauch, Mapping basement magnetitation zones from aeromagnetic data in the san juan basin, New Mexico, in *1982 SEG Annual Meeting, SEG 1982*, pp. 246–247, Society of Exploration Geophysicists, doi:10.1190/1.0931830346.ch16, 1982.

Davidson, J. P., D. J. Morgan, B. L. Charlier, R. Harlou, and J. M. Hora, Microsampling and isotopic analysis of igneous rocks: Implications for the study of magmatic systems, *Annual Review of Earth and Planetary Sciences*, *35*, 273–311, doi:10.1146/annurev.earth.35.031306.140211, 2007.

de Groot, L. V., K. Fabian, I. A. Bakelaar, and M. J. Dekkers, Magnetic force microscopy reveals meta-stable magnetic domain states that prevent reliable absolute palaeointensity experiments, *Nature Communications*, *5*(1), 1–10, doi:10.1038/ncomms5548, 2014.

de Groot, L. V., K. Fabian, A. Béguin, P. Reith, A. Barnhoorn, and H. Hilgenkamp, Determining Individual Particle Magnetizations in Assemblages of Micrograins, *Geophysical Research Letters*, *45*(7), 2995–3000, doi:10.1002/2017GL076634, 2018.

de Groot, L. V., et al., Micromagnetic Tomography for Paleomagnetism and Rock-Magnetism, *Journal of Geophysical Research: Solid Earth*, *126*(10), e2021JB022,364, doi:10.1029/2021JB022364, 2021.

Dunlop, D. J., and Ö. Özdemir, *Rock Magnetism Fundamentals and Frontiers*, 573 pp., Cambridge University Press, doi:10.1017/cbo9780511612794, 1997.

Fabian, K., and L. V. De Groot, A uniqueness theorem for tomography-assisted potential-field inversion, *Geophysical Journal International*, *216*(2), 760–766, doi:10.1093/GJI/GGY455, 2019.

Farchi, E., Y. Ebert, D. Farfurnik, G. Haim, R. Shaar, and N. Bar-Gill, Quantitative Vectorial Magnetic Imaging of Multi-Domain Rock Forming Minerals Using Nitrogen-Vacancy Centers in Diamond, *SPIN*, *7*(3), 1740,015, doi:10.1142/S201032471740015X, 2017.

Fu, R. R., E. A. Lima, M. W. Volk, and R. Trubko, High-Sensitivity Moment Magnetometry With the Quantum Diamond Microscope, *Geochemistry, Geophysics, Geosystems*, *21*(8), e2020GC009,147, doi:10.1029/2020GC009147, 2020.

Glenn, D. R., R. R. Fu, P. Kehayias, D. Le Sage, E. A. Lima, B. P. Weiss, and R. L. Walsworth, Micrometer-scale magnetic imaging of geological samples using a quantum diamond microscope, *Geochemistry, Geophysics, Geosystems*, *18*(8), 3254–3267, doi:10.1002/2017GC006946, 2017.

Lima, E. A., and B. P. Weiss, Obtaining vector magnetic field maps from single-component measurements of geological samples, *Journal of Geophysical Research: Solid Earth*, *114*(6), 6102, doi:10.1029/2008JB006006, 2009.

Lima, E. A., B. P. Weiss, L. Baratchart, D. P. Hardin, and E. B. Saff, Fast inversion of magnetic field maps of unidirectional planar geological magnetization, *Journal of Geophysical Research: Solid Earth*, *118*(6), 2723–2752, doi:10.1002/jgrb.50229, 2013.

Lima, E. A., A. C. Bruno, H. R. Carvalho, and B. P. Weiss, Scanning magnetic tunnel junction microscope for high-resolution imaging of remanent magnetization fields, *Measurement Science and Technology*, *25*(10), 105,401, doi:10.1088/0957-0233/25/10/105401, 2014.

McElhinny, M. W., and L. P. McFadden, Rock Magnetism, in *Paleomagnetism*, edited by M. W. McElhinny and L. P. McFadden, pp. 31–77, Academic Press, doi:10.1016/S0074-6142(00)80095-9, 2000.

Nagy, L., W. Williams, A. R. Muxworthy, K. Fabian, T. P. Almeida, P. Ó. Conbhuí, and V. P. Shcherbakov, Stability of equidimensional pseudo–single-domain magnetite over billion-year timescales, *Proceedings of the National Academy of Sciences*, *114*(39), 10,356–10,360, doi:10.1073/PNAS.1708344114, 2017.

Néel, L., Theorie du trainage magnetique des ferromagnetiques en grains fins avec applications aux terres cuites, *Ann. Geophys.*, *5*, 99–136, 1949.

Néel, L., Some theoretical aspects of rock-magnetism, *Advances in Physics*, *4*(14), 191–243, doi:10.1080/00018735500101204, 1955.

Nichols, C. I., J. F. Bryson, J. Herrero-Albillos, F. Kronast, F. Nimmo, and R. J. Harrison, Pallasite paleomagnetism: Quiescence of a core dynamo, *Earth and Planetary Science Letters*, *441*, 103–112, doi:10.1016/j.epsl.2016.02.037, 2016.

Oliveira Jr., V. C., D. P. Sales, V. C. Barbosa, and L. Uieda, Estimation of the total magnetization direction of approximately spherical bodies, *Nonlinear Processes in Geophysics*, *22*(2), 215–232, doi:10.5194/npg-22-215-2015, 2015.

O'Reilly, W., Applications of rock and mineral magnetism, in *Rock and Mineral Magnetism*, pp. 194–212, Springer US, doi:10.1007/978-1-4684-8468-7_9, 1984.

Reid, A. B., J. M. Allsop, H. Granser, A. J. Millett, and I. W. Somerton, Magnetic interpretation in three dimensions using Euler deconvolution, *GEOPHYSICS*, *55*(1), 80–91, doi:10.1190/1.1442774, 1990.

Tauxe, L., S. Banerjee, R. F. Butler, and R. Van der Voo, tauxe Essentials of Paleomagnetism: Fifth Web Edition, 2018.

Thompson, D. T., EULDPH: a new technique for making computer-assisted depth estimates from magnetic data., *Geophysics*, *47*(1), 31–37, doi:10.1190/1.1441278, 1982.

van der Walt, S., J. L. Schönberger, J. Nunez-Iglesias, F. Boulogne, J. D. Warner, N. Yager, E. Gouillart, and T. Yu, scikit-image: image processing in Python, *PeerJ*, *2*, e453, doi:10.7717/peerj.453, 2014.

Verberne, R., S. M. Reddy, D. W. Saxey, D. Fougerouse, W. D. Rickard, D. Plavsa, A. Agangi, and A. R. Kylander-Clark, The geochemical and geochronological implications of nanoscale trace-element clusters in rutile, *Geology*, *48*(11), 1126–1130, doi:10.1130/G48017.1, 2020.

Weiss, B. P., E. A. Lima, L. E. Fong, and F. J. Baudenbacher, Paleomagnetic analysis using SQUID microscopy, *Journal of Geophysical Research: Solid Earth*, *112*(9), 9105, doi:10.1029/2007JB004940, 2007.